Multi-module series suppressor for the protection of wind farm transformers against resonance overvoltages

Heidary, Amir; Niasar, Mohamad Ghaffarian; Popov, Marjan

DOI
10.1016/j.ijepes.2025.111090

Publication date
2025

Document Version
Final published version

Published in
International Journal of Electrical Power and Energy Systems

Electrical Power and Energy Systems 172 (2025) 111090

Contents lists available at ScienceDirect

International Journal of Electrical Power and Energy Systems

journal homepage: www.elsevier.com/locate/ijepes

Multi-module series suppressor for the protection of wind farm transformers against resonance overvoltages

Amir Heidary *, Mohamad Ghaffarian Niasar, Marjan Popov

Delft University of Technology, Faculty of EEMCS, Mekelweg 4, 2628CD Delft, The Netherlands

ARTICLE INFO

Keywords:
Wind farm
Transformer
Series suppressor
Resonance
Overvoltage
Transient

ABSTRACT

Large-scale integration of renewable energy sources (RESs) presents significant challenges for modern power grids, particularly with wind farms playing a crucial role in energy generation. However, frequent switching operations during the (dis)connection of wind farms and lightning strikes on wind turbines can induce severe transient overvoltages. These fast transients (FTs) pose a serious risk to wind farm substations, potentially compromising the reliability of renewable energy generation. In particular, protecting wind farm transformers from FTs, resonances, and resulting overvoltages is essential for ensuring stable operation. This paper proposes a modular series transient suppressor (MSTS) designed to enhance the protection of wind farm transformers against FTs, thereby improving system reliability. The MSTS consists of multiple resonant circuit modules, including a core, a low-voltage capacitor, and a resistor connected in series with the transformer. Its operational behavior is analyzed using analytical methods and validated through simulation studies. Furthermore, experimental testing performed on a developed MSTS prototype confirms its effectiveness in mitigating transient overvoltages for a wind farm transformer model circuit at a 60 kV transient voltage level.

1. Introduction

Lightning strikes in power systems generate fast transients (FTs) that propagate through the network, posing a significant risk to power equipment [1]. Additionally, the integration of renewable energy sources (RESs) such as wind farms, the use of more compact substations, and switching operations in power grid management contribute to the frequent occurrence of FTs in modern power systems [2,3]. These transients can severely impact crucial equipment within wind farms, particularly transformers, leading to resonance and overvoltage conditions [4], which can be detrimental to both transformer windings and wind generators. The harmonic content of FTs may resonate with wind farm transformer windings, compromising insulation integrity and increasing the risk of damage [5].

Wind farm transformer protection, as an essential component of the power system, requires the application of effective protection devices [6]. Various methods have been employed to safeguard wind farm transformers from FTs, including surge arresters [7], surge capacitors, RC snubbers [8], ZnO-RC (ZORC) [9], pre-insertion resistors (PIR) [10], frequency-dependent devices (FDD) [11,12], and chokes [13,14]. However, many of these methods have limitations related to voltage level, operational delays, and the inability to filter a wide range of harmonic frequencies effectively. Most of these solutions do not fully address internal resonance overvoltage matters, especially for wind farm transformers [15]. Although wind turbines and other equipment are often equipped with flashover devices or surge arresters, transient overvoltages can still propagate due to:

- Incomplete dissipation of high-frequency transient energy within the short suppression time
- Device failure when transient energy exceeds rated capability
- Residual high-frequency components after voltage clipping by surge arresters, which can excite transformer resonance
- Induced transients from nearby lightning without a direct strike.

Recent research explored new approaches to wind farm transformer protection, such as adding a series suppressor to the wind farm transformer coil model, which has shown promising results [16]. Another research work examined the use of a tuned choke with a resonance capacitor connected to the secondary winding of the choke [17]. Further research introduced the concept of adding multiple toroid cores to the guard wire of transmission lines, which successfully enhanced

* Corresponding author.
E-mail addresses: A.heidary@tudelft.ni, Amir.powersys@gmail.com (A. Heidary).

https://doi.org/10.1016/j.ijepes.2025.111090
Received 18 April 2025; Received in revised form 14 August 2025; Accepted 4 September 2025
Available online 12 September 2025

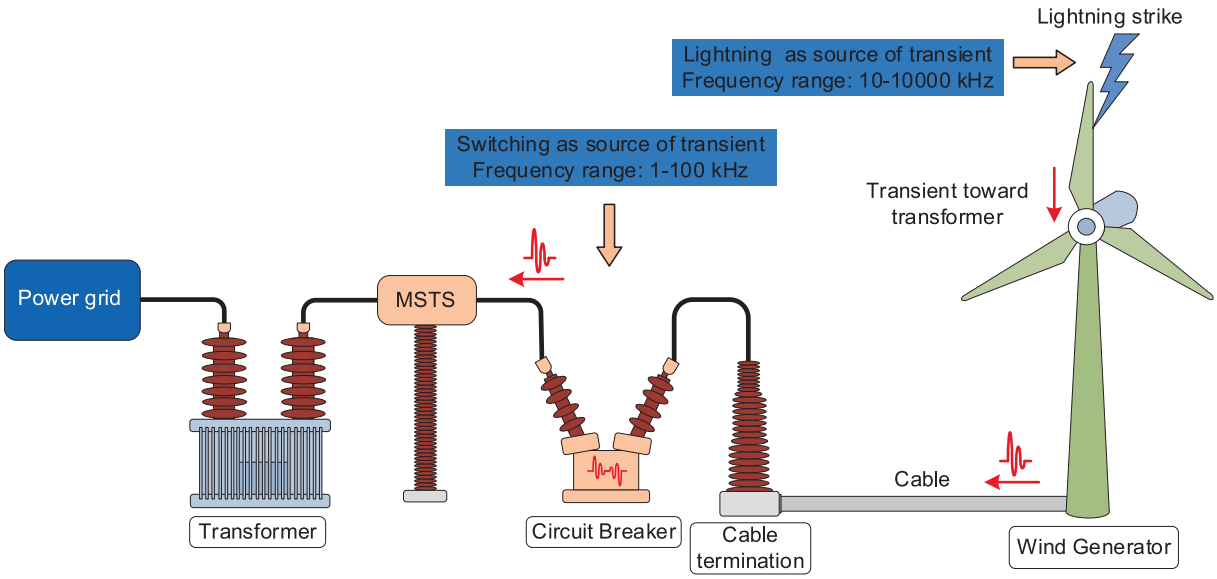

Fig. 1. MSTS integration with wind farm transformer substation.

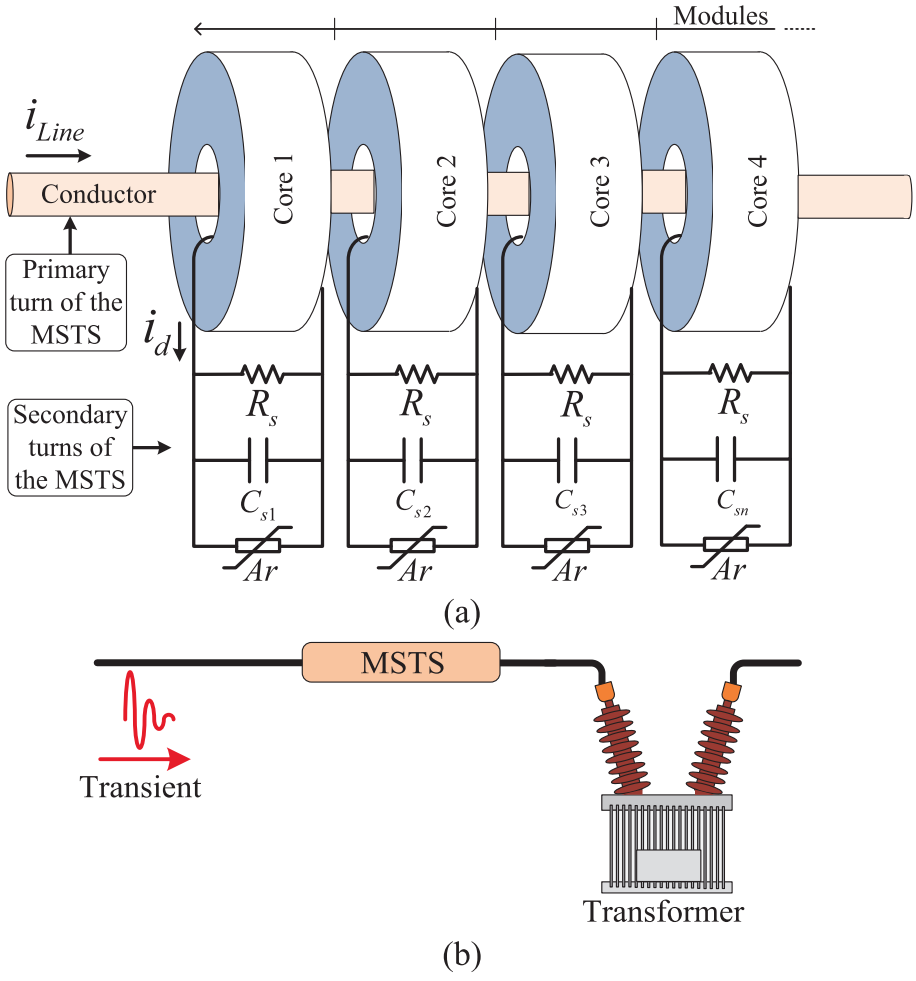

Fig. 2. (a) MSTS structure, (b) configuration in series with a wind farm transformer.

protection [18].

Despite these advancements, there remains a need for a protection device that can provide significant impedance over a wide frequency range while withstanding high voltage stresses [19].

This paper proposes a modular series transient suppressor (MSTS) as an effective solution for protecting wind farm transformers against fast transient signals. The MSTS is designed as a general-purpose resonance suppression device capable of protecting all types of power transformers

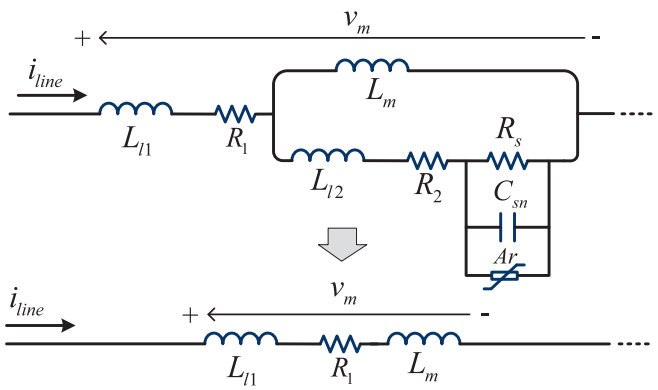

Fig. 3. Equivalent circuit of an MSTS module for nominal frequencies.

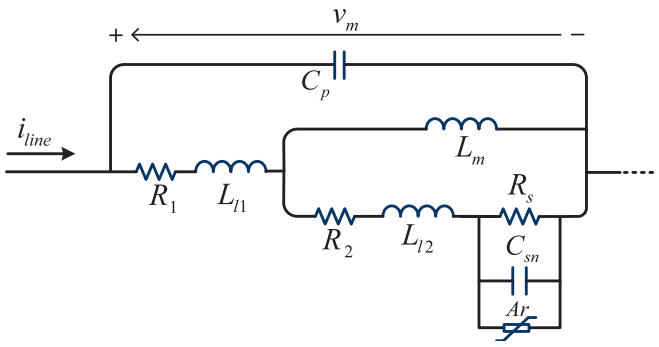

Fig. 4. MSTS High-frequency equivalent model.

from resonance overvoltages. However, wind farm transformers are more frequently subjected to transient phenomena. The MSTS offers the following key advantages:

- Operation over a wide frequency range.
- Ability to withstand high voltage stress.
- Modular design to accommodate higher voltage levels.
- Use of resonance frequency shifting in each module.
- Multilayer core design to prevent saturation.

The performance of the MSTS is analyzed using Finite Element Method (FEM) simulations and Electromagnetic Transients Program (EMTP) simulations, and is further validated through experimental testing.

The paper is organized as follows: Section 2 describes the operation and configuration of the MSTS. Section 3 presents the fundamental formulas that define the MSTS's operational principles. Section 4 presents the simulation results, while Section 5 discusses the experimental evaluation. Section 6 discusses the MSTS benefits based on a comparison study, and finally, Section 7 provides meaningful conclusions.

2. MSTS configuration, description, and analysis

Modular Series Transient Suppressor (MSTS) is a protection device connected in series with the wind farm transformer, as shown in Fig. 1, to mitigate resonance overvoltages. Functioning as a series filter for transient signals, the MSTS is designed to attenuate critical frequency components within an acceptable range, reducing the impact of transient phenomena such as wind generator switching operations or lightning strikes on wind turbine towers. Although there are variety of transient phenomena, such as transient recovery voltage or ultra short impulses, lightning strikes to wind turbine towers or switching events occurring in wind generators are primary sources of transients containing high-frequency components (several hundred kHz).

The attenuation of these components depends on system configuration, cable characteristics, and component impedances. Within wind farm collector systems, such frequencies can propagate efficiently over short to medium distances and may excite transformer internal resonance. This is the primary hazard addressed in our study. The structure and configuration topology of the MSTS are illustrated in Fig. 2.

From Fig. 2 (a), it is apparent that MSTS is a modular device for which each module comprises a toroid core on a power line cable (considered as one turn), a secondary turn (one turn), a resistor R_s, a capacitor C_s, and an arrester A_r. Indeed, the only difference between each module is the capacitance of the secondary side of the MSTS (C_s), with the value shifted in a certain range to shift the impedance character of each module. In this structure, the toroid core is applied around the main conductor of the power line, where that piece of the conductor is known as the primary turn of the series protection device. Furthermore, the secondary turn is connected to the parallel suppressor resistor, resonance capacitor, and arrester. Fig. 2 (b) illustrates that the overall MSTS circuit is a series device connected to the wind farm transformer terminal. The operation of the MSTS is investigated for two scenarios: nominal frequency operation and operation in response to transient signals.

2.1. MSTS operation in power grid normal operation

During nominal power grid operation, no transient signals are present. Therefore, the low-frequency equivalent of the coupled inductor can be used to analyze the MSTS operation. An equivalent circuit is shown in Fig. 3.

The impedance value of the secondary circuit (including the resistor in the range of kiloohms and the capacitor in the range of nanofarads) is much larger than the magnetization inductance L_m. Therefore, the equivalent circuit is simplified, encompassing the leakage inductance of a short piece of power cable or line that passes through the cores, the MSTS module's magnetization inductance, and the cable section's resistance that passes through the cores. By assuming (1), the impedance of the MSTS in series with a line can be expressed by equation (2), where n refers to the number of modules.

$$j\omega L_m << R_2 + j\omega L_{l2} + \left(R_s \| 1/j\omega C_s \| R_{Ar}\right) \tag{1}$$

$$Z_m = n(R_1 + j\omega(L_{l1} + L_m)) \tag{2}$$

The impedance Z_m of the MSTS, as obtained by (2), is a small value at power frequency. Therefore, the voltage drop computed by (3) can be ignored. The impedance is roughly similar to the cable impedance (here, the impedance is likely to be the impedance of several meters of the cable), and the voltage drop is nearly zero.

$$V_m = I_{line}.n(R_1 + j\omega(L_{l1} + L_m)) \tag{3}$$

In addition, the power loss of the MSTS P_{loss} is negligible during normal operations, as computed by (4).

$$P_{loss} = nR_1(I_{line})^2 \tag{4}$$

The calculated power loss in (4) results in a negligible temperature rise, comparable to that of an overhead line under steady-state conditions.

2.2. Operation during transient oscillations

In this section, it is assumed that the transient signal contains high-frequency oscillations passing through the MSTS. Therefore, the high-frequency equivalent circuit of the MSTS is considered. This equivalent circuit is illustrated in Fig. 4.

The circuit has several resonance frequencies depending on the value of the connected capacitor (C_{sn}) to the secondary side of each module of MSTS. The equivalent circuit of one module of MSTS is illustrated in

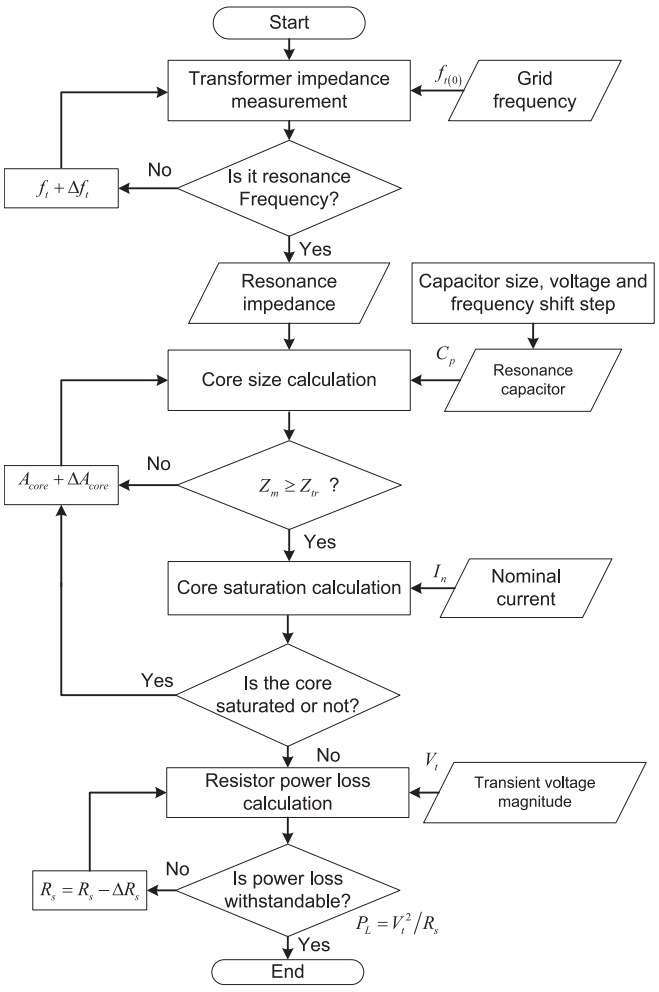

Fig. 5. MSTS design algorithm.

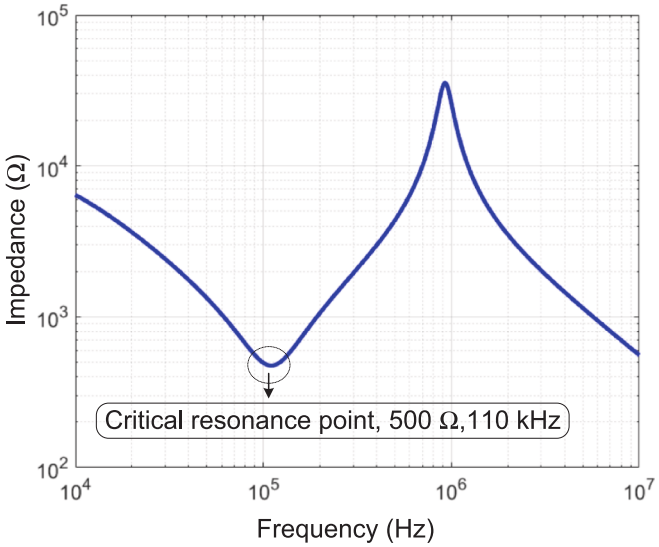

Fig. 6. Harmonic impedance of an equivalence wind farm transformer.

Fig. 4. The notable feature of the MSTS is its ability to provide significant overall impedance against critical harmonics of transient signals, where its impedance is the sum of the module's impedance around its resonance point. This resonance frequency, which provides exceptionally high impedance in series with the wind farm transformer, is due to the resonance occurring between the magnetizing inductance L_m of each module and the capacitances (C_{sn}) of the secondary side of each module of the MSTS. This resonance frequency is tuneable by changing the value of the external capacitance in the secondary circuit. The impedance of the MSTS is computed as presented in (5), where m refers to the number of modules needed to develop the MSTS.

Table 1.P
Arameters and features of the simulated msts.

Module	L_m	L_{l1}	L_{l2}	R_1	R_2	R_S	C_{sn}	C_p
1,2	72 μH	0.25 μH	0.2 μH	4 mΩ	8 mΩ	98 Ω	15 nF	18 pF
3,4,5	72 μH	0.25 μH	0.2 μH	4 mΩ	8 mΩ	98 Ω	22 nF	18 pF
6,7,8	72 μH	0.25 μH	0.2 μH	4 mΩ	8 mΩ	98 Ω	33 nF	18 pF
9,10	72 μH	0.25 μH	0.2 μH	4 mΩ	8 mΩ	98 Ω	50 nF	18 pF

Table 2
Parameters of the unified core MSTS module.

Parameter	description	Value
l_c	Length of the core	25 mm
l_{cc}	Length of the core side	110 mm
l_{di}	The inner diameter of the core	20 mm
l_{do}	The outer diameter of the core	130 mm
D	The outer radius of the core	65 mm
d	The inner radius of the core	10 mm
A_p	Primary wire cross-section	2 mm^2
A_s	Secondary wire cross-section	1 mm^2
μ_c	Magnetic permeability	4000
B_m	Maximum magnetic flux density	1.2 T

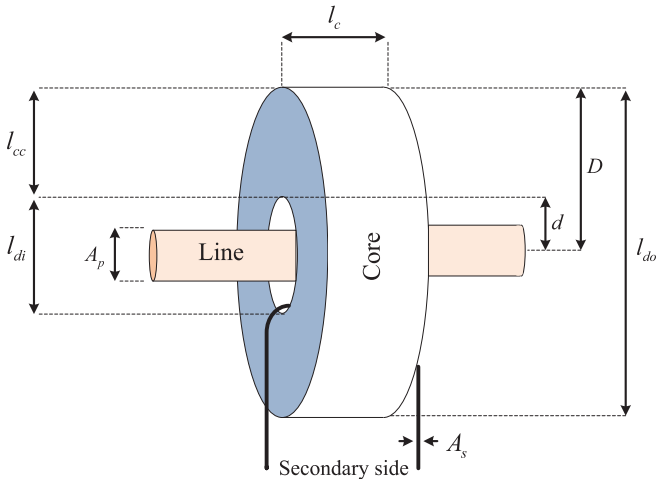

Fig. 7. MSTS module geometry.

$$Z_m = \sum_{m=1}^{n} \left(1/\omega C_p\right) \| \left(R_1 + j\omega L_{l1} + \left(j\omega L_m \| \left(R_2 + j\omega L_{l1} + \left(1/\omega C_{sn} \| R_s\right)\right)\right)\right) \quad (5)$$

By carrying out the frequency sweep analysis for $\omega = 2\pi f$ within the nominal frequency ($f = 50$ Hz) and the maximum studied frequency in (5), the frequency response of MSTS can be obtained during the frequency sweep domain. Furthermore, the power loss of the connected resistors at the secondary side of MSTS modules can be computed by (6), and the total dissipated energy W_m in the resistor by (7).

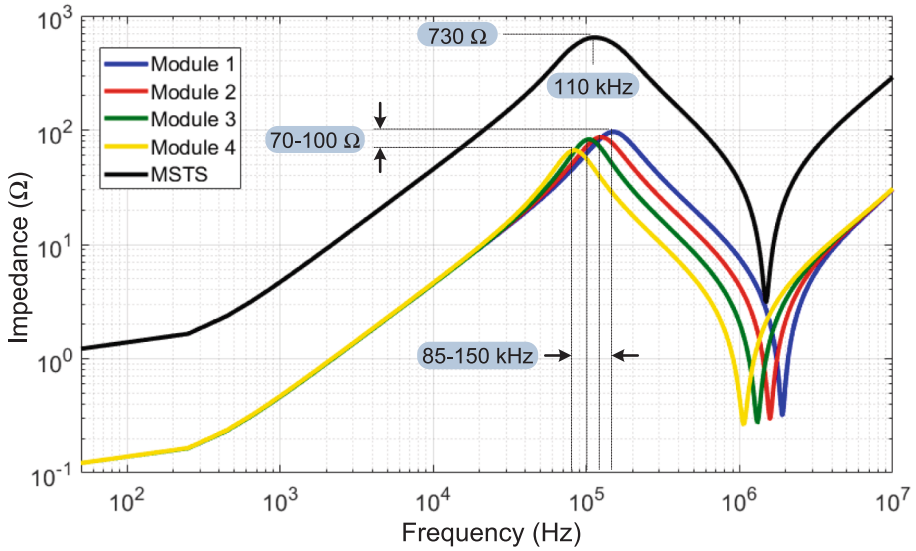

Fig. 8. Impedance character of MSTS simulated model.

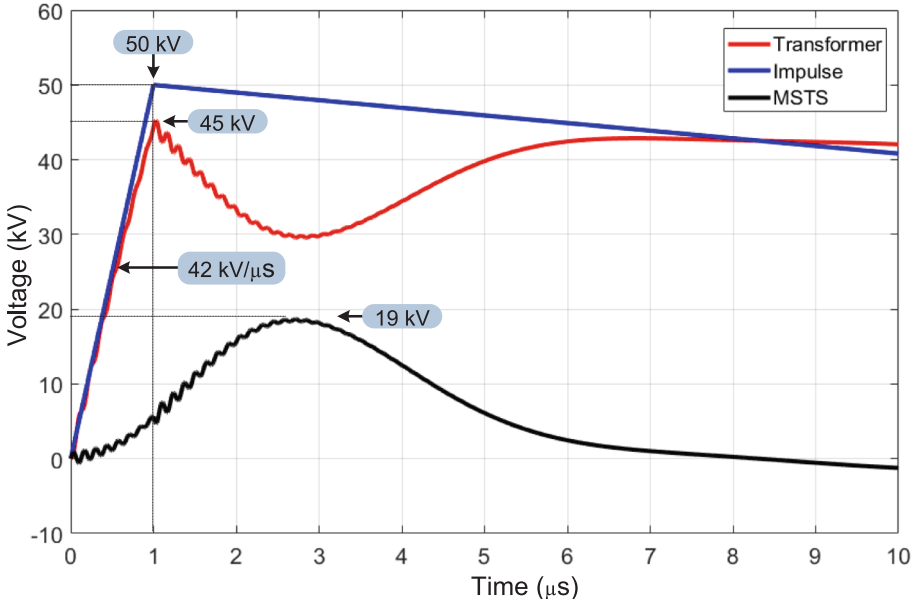

Fig. 9. Impulse time domain simulation of protected wind farm transformer with MSTS.

$$P_{loss} = n\left((v_s(t))^2/R_s\right) \tag{6}$$

$$W_m = n\int_0^t \left((v_s(t))^2/R_s\right)dt \tag{7}$$

where t refers to the duration of the transient signal and v_s is the secondary-side voltage, which is the sum of the secondary voltage of each mode as shown in (8). Since this energy is distributed among the modules, the temperature rise during the short transient period remains small and is easily controlled.

$$v_s = v_{m1} + v_{m2} + \ldots + v_n \tag{8}$$

2.3. Parameter calculation of MSTS

The most critical data for parameter determination of the MSTS is the wind farm transformer's critical resonance frequency range and its impedance around the resonance frequency. It is crucial that the impedance of the MSTS for this frequency range is comparable with the wind farm transformer impedance, to be able to suppress the voltage magnitude at the wind farm transformer terminal. The algorithm of the MSTS is illustrated in Fig. 5.

In this algorithm, the first step is to perform a wind farm transformer impedance sweep measurement starting from the grid frequency. This sweep identifies the resonance point and the wind farm transformer impedance (Z_{tr}) at the critical resonance frequency. The character of the wind farm transformer model is illustrated in Fig. 5. This simplified model reflects the wind farm transformer's critical resonance based on the wind farm transformer RLC disk model, which is elaborated on in [16]. Then, by considering the resonance capacitor (C_{sn}) specifications based on the constraints of sizing and voltage, the core cross-section is computed to satisfy the requirement $Z_m \geq Z_{tr}$. In the next step, the core cross-section is recalculated based on the nominal current of the power line to ensure that it operates well below the core saturation region. Ultimately, the secondary-connected resistor R_2, acting as a damper, is selected by considering the maximum possible power dissipation p_{loss}

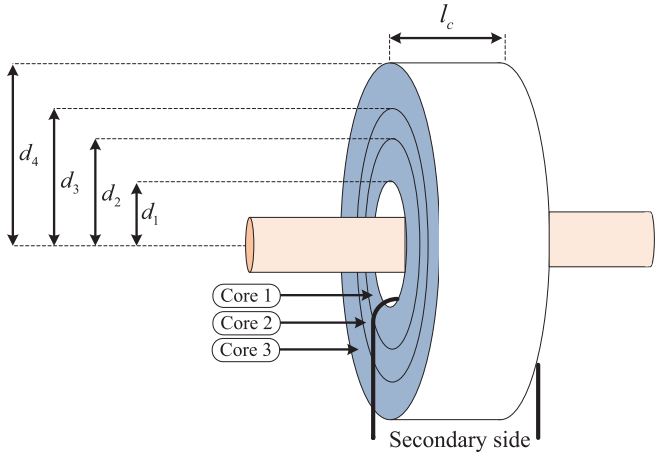

Fig. 10. Geometry of a multilayer core module.

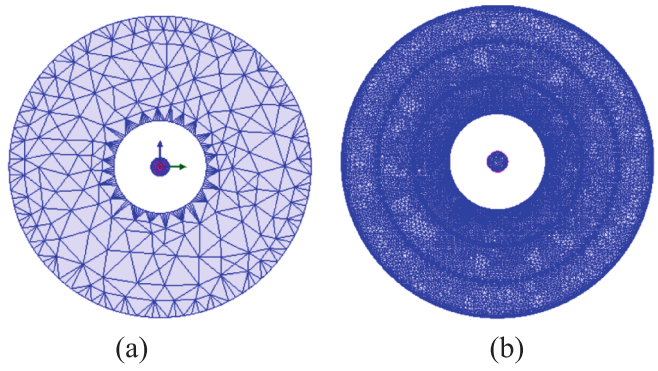

Fig. 11. Applied FEM meshes for module geometry a) unified core, b) multilayer core.

$_{(max)}$. The arrester in the secondary circuit does not engage during normal operation; its primary function is to protect the resonance capacitor from overvoltage, with its operating voltage set equal to the capacitor's maximum voltage Fig. 6.

On the other hand, optimization techniques such as genetic algorithms or particle swarm optimization could further refine these parameters. However, in the MSTS parameter calculation, the objective was to demonstrate the fundamental design approach. The calculated fundamental RLC parameters satisfy the constraints, though they could be further improved through optimization algorithms in future stages of this research.

3. The MSTS simulation in EMTP software

The model of the designed MSTS, as shown in Fig. 4, is implemented in EMTP for further evaluation. The simulated MSTS consists of 10 modules, with the characteristics of each module group as shown in Table 1. The main parameters are calculated based on the algorithm depicted in Fig. 5. The wind farm transformer's resonance frequency spans from 100 to 120 kHz, with a resonance impedance (Z_{tr}) of approximately 500 Ω. The selected resonance capacitor of the MSTS secondary side (C_{sn}) varies from 10 to 60 nF at 5 kV. The magnetization inductance (L_m) and secondary resistor (R_s) can be determined based on the equivalent circuit to satisfy the constraint, which is $Z_m \geq Z_{tr}$. The remaining parameters are functions of the module geometry, calculated using the method described in [18].

As shown in Table 1, the studied MSTS consists of ten different modules, with some modules sharing identical parameters to enhance the overall impedance of the MSTS near the resonance frequencies of the modules.

The geometry data of the MSTS is presented in Table 2, and the associated parameters are provided in Fig. 7.

3.1. Frequency sweep simulation of MSTS

The simulation is carried out for the frequency response of the MSTS over the studied frequency range. This simulation aims to extract the characteristics of the MSTS across a wide range of frequencies (50 Hz to 10 MHz) to assess its impact on the wind farm transformer's critical resonance frequency (100—120 kHz). The resulting impedance sweep curves are presented in Fig. 8.

The MSTS terminal frequency sweep (FS) shows that the impedance of the MSTS exceeds 500 Ω within the 80–180 kHz range, peaking at nearly 800 Ω (black curve, Fig. 8). This peak results from the combined effects of each module within the MSTS. The system's overall resonance occurs around 110 kHz, while the individual resonance frequencies of modules 1, 2, 3, and 4 are 85 kHz, 101 kHz, 120 kHz, and 150 kHz, respectively. At these resonance points, the impedance of each module ranges between 70 and 100 Ω. Based on the MSTS design specifications, the second resonance point, where the impedance is minimized, occurs above 1 MHz. This frequency is far from the resonance point of the wind farm transformer and does not affect its operational frequency range. The designed MSTS matches well the resonance frequency of the wind farm transformer.

3.2. Impulse time domain simulation of MSTS

The simulation test setup consists of an MSTS connected in series to a wind farm transformer represented by a simplified model with a resonance frequency of 105 kHz, and a resonance impedance of 500 Ω, as shown in Fig. 2(b). The simulation evaluates the MSTS's performance in limiting the transient voltage's frequency content at the operating frequency and suppressing the overall magnitude of the transient signal. The excitation source is a lightning transient signal, with its specifications shown in Fig. 9 as the blue curve. Following the excitation, the black curve illustrates the voltage drop across the MSTS, while the red curve shows the voltage at the wind farm transformer terminal.

As shown in Fig. 9, the MSTS demonstrates a significant voltage drop in response to the impulse transient. The effects are evident in the reduced peak voltage and RMS voltage at the wind farm transformer terminal, as well as in the rate of rise of the voltage (RRV). Specifically, the peak voltage at the wind farm transformer terminal is 45 kV, which is 5 kV lower than the 50 kV peak of the impulse source, while the RRV is reduced to 42 kV/μs from the original value, which is 50 kV/μs. The peak voltage across the MSTS, acting as a suppressor, also reaches 19 kV. This simulation confirms that the designed MSTS effectively reduces the magnitude and RRV of the transient signal at the wind farm transformer terminal, thereby eliminating the harmonic content's magnitude.

4. The MSTS magnetic flux field study

In this section, the distribution of the magnetic flux density in the MSTS core is discussed and the effect of saturation is addressed, which is a critical concern for series-connected inductors [20]. The primary challenge lies in the non-uniform distribution of the magnetic flux density in the toroidal core, causing saturation in areas near the primary winding; as such, the performance of the MSTS core is reduced. A new solution to mitigate this phenomenon is utilizing a multilayer core instead of a unified toroid core. This multilayer design constrains the magnetic flux distribution, ensuring uniformity and preventing core saturation.

The effectiveness of this solution is demonstrated through simulations by using finite element method (FEM) analysis. The redesigned MSTS's inductance is also evaluated to confirm the improvements. In the first step, the geometry of the MSTS module is modelled by FEM, with

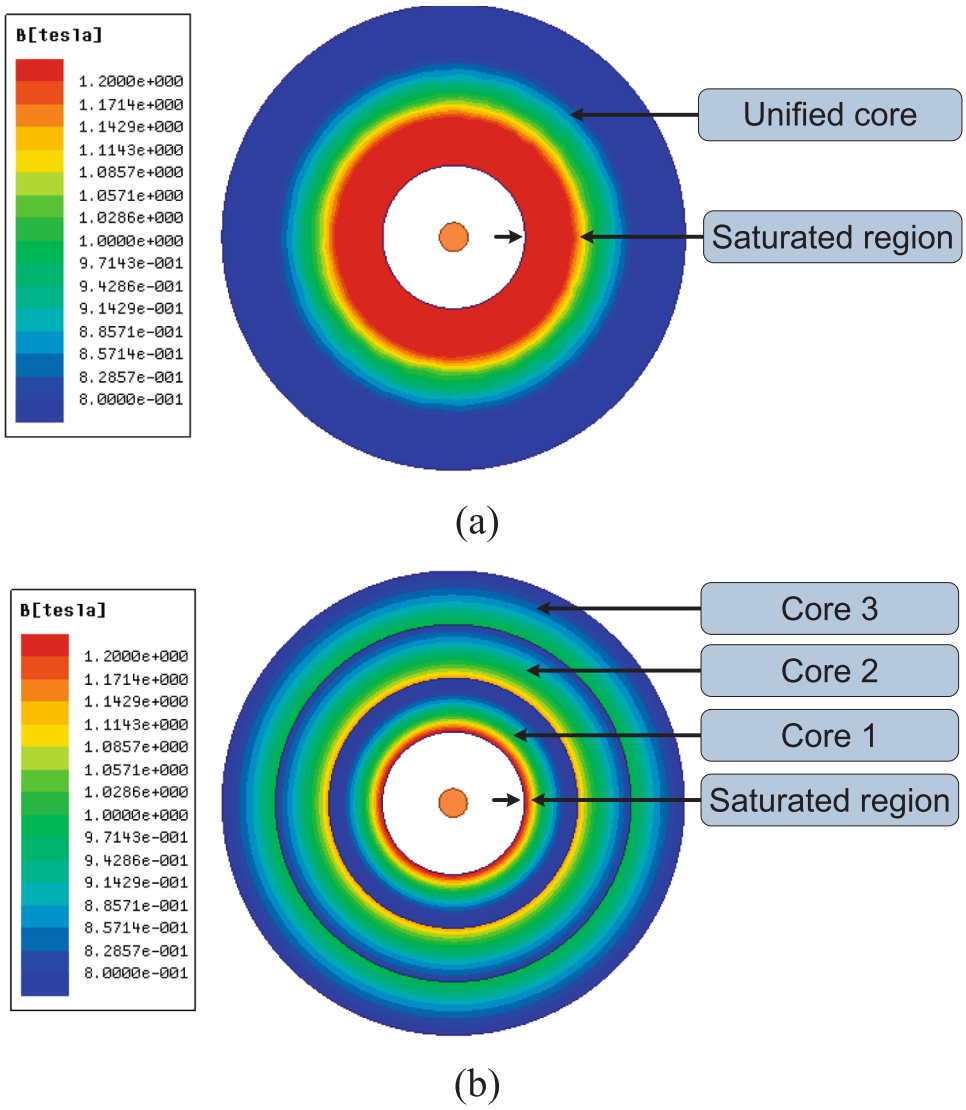

Fig. 12. A) magnetic flux density in unified core, b) magnetic flux density in multilayer core.

Table 3
Magnetic and geometric parameters of the multilayer core MSTS module.

Parameter	description	Value
l_c	Length of the core	25 mm
d_1	The inner radius of the core 1	10 mm
d_2	The outer radius of the core 1	25 mm
d_3	The outer radius of the core 2	50 mm
d_4	The outer radius of the core 3	65 mm
μ_{c1}	Magnetic permeability (core 1)	2500
μ_{c2}	Magnetic permeability (core 2)	4000
μ_{c3}	Magnetic permeability (core 3)	5000
B_m	Maximum magnetic flux density	1.2 T

meshing applied accordingly. Next, the mathematical constraints governing each core layer's characteristics are discussed. Finally, the magnetic flux distribution and saturation status are analysed, as illustrated in Fig. 10.

4.1. Geometry design and constraints of MSTS

The maximum flux density of the core is a key constraint for ensuring the proper operation of the designed MSTS. Typically, commercially available cores operate within a range of 0.1 T to over 2 T. For the MSTS design, the maximum magnetic flux density of the cores is set at 1.2 T. Additionally, the required magnetization inductance for each module, with one turn as the primary winding, is 72 μH, as shown in Table 1. Consequently, the overall core cross-section can be determined based on the magnetic permeability. The core specification in the linear state is calculated as follows (where L_{uc} represents the inductance of the module when the core is uniform).

$$L_{uc} = \frac{\mu_{uc} l_c}{\pi} \left(\frac{D-d}{D+d} \right) \tag{9}$$

In (9), μ_{uc} represents the magnetic permeability of the unified core, and other geometrical parameters are defined in Fig. 5 and Table 2. To improve the magnetic distribution in the unified core module, the inductance of the multilayer scheme module should match that of the unified core module. However, the geometry, number of layers, and magnetic permeability of the cores should be adjusted. The next constraint is presented in (10), which shows that the inductance of the unified core module is equal to the sum of inductances generated by each core layer (L_{c1}, L_{c2}, and L_{c3}). Here, the number of layers is considered to be three.

$$L_{uc} = L_{c1} + L_{c3} + L_{c3} \tag{10}$$

The geometry of the multilayer modules is depicted in Fig. 10.

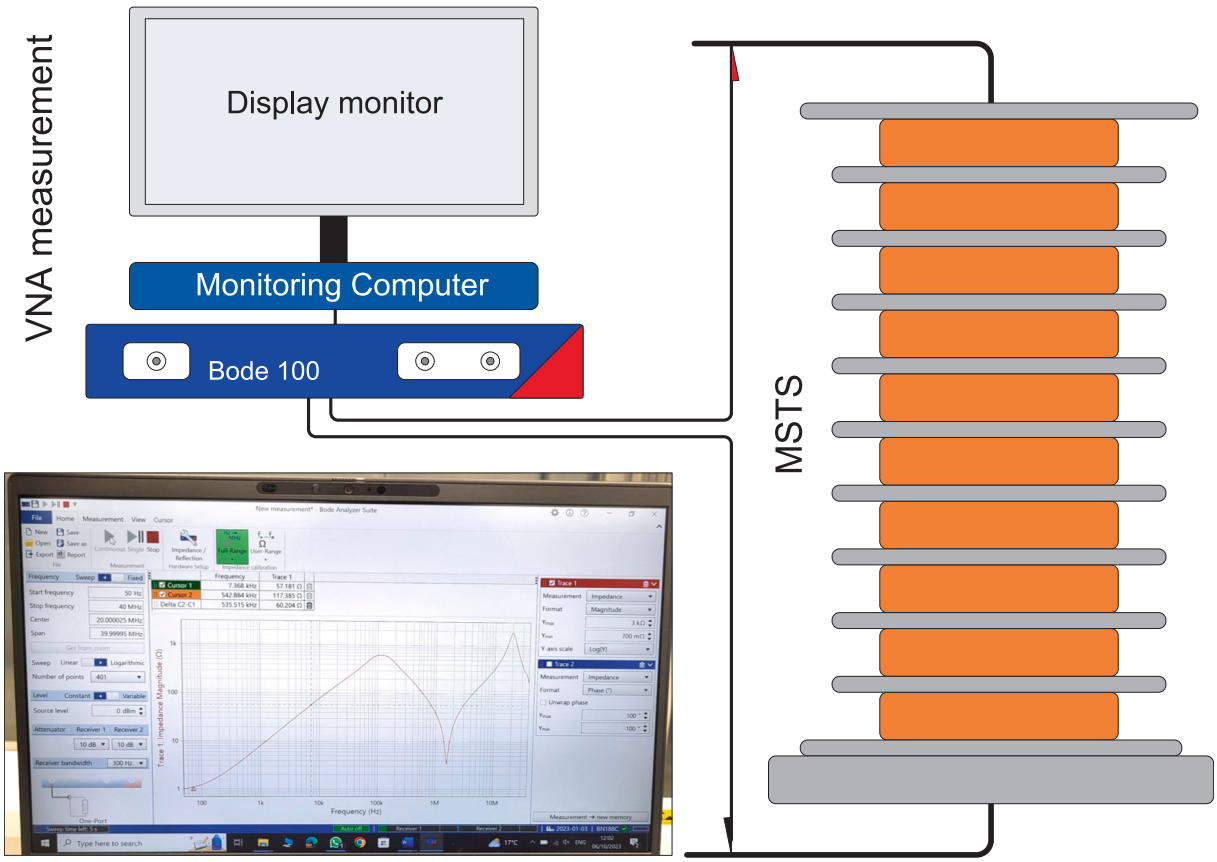

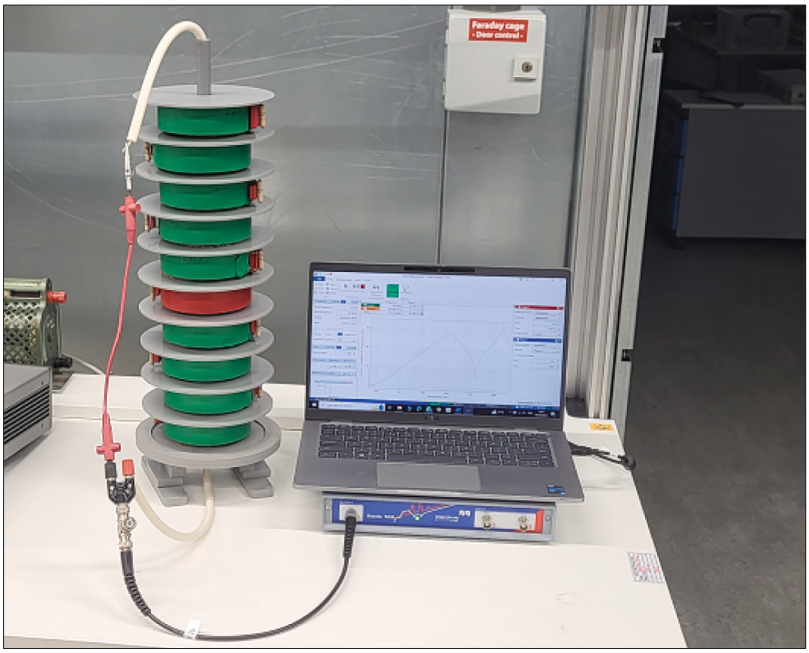

Fig. 13. Impedance frequency response measurement setup of MSTS.

By considering the geometry parameters, the inductance of each core is calculated by (11), (12), and (13), ensuring that all three inductances are equal, as shown by (14).

$$L_{c1} = \frac{\mu_{c1} l_c}{\pi} \left(\frac{d_2 - d_1}{d_2 + d_1} \right) \tag{11}$$

$$L_{c2} = \frac{\mu_{c2} l_c}{\pi} \left(\frac{d_3 - d_2}{d_3 + d_2} \right) \tag{12}$$

$$L_{c3} = \frac{\mu_{c3} l_c}{\pi} \left(\frac{d_4 - d_3}{d_4 + d_3} \right) \tag{13}$$

$$L_{c1} = L_{c2} = L_{c3} \tag{14}$$

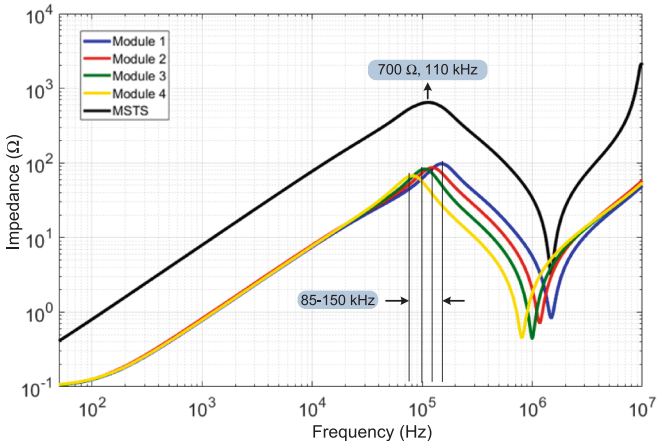

Fig. 14. Harmonic impedance measurement results of MSTS.

To satisfy equation (14), condition (15) must be met, while for the geometry, the constraint expressed by (16) should hold where the length of each module core is (l_c) the same.

$$\mu_{c1} < \mu_{c2} < \mu_{c3} \tag{15}$$

$$\left(\frac{d_2 - d_1}{d_2 + d_1}\right) > \left(\frac{d_2 - d_1}{d_2 + d_1}\right) > \left(\frac{d_2 - d_1}{d_2 + d_1}\right) \tag{16}$$

With constraints (9), (14), and (15), these two geometries are designed and meshed in a FEM model, as illustrated in Fig. 11 (a) and (b). The primary objective is to compare the unified core and the multilayer core modules in terms of magnetic flux density distribution and saturation behaviour.

4.2. Magnetic flux study in the modules' core

In this subsection, the magnetic flux analysis focuses on the two described configurations: the unified core and the multilayer core. Both concepts for magnetic flux density are plotted and presented in Fig. 12 (a) and (b). The features of the unified core concept are presented in Table 2, and the multilayer simulated concept data are represented in Table 3.

As shown in Fig. 12(a), when the primary conductor of the unified core module is excited with 100 A current (consistent with the designed scale of the prototype), a significant portion of the toroidal core near the wire becomes saturated. This saturation affects approximately 25 mm of the core, significantly reducing each module's performance in the MSTS system. The inductance of the module before being saturated is approximately 72 μH, and it drops to 42 μH after saturation.

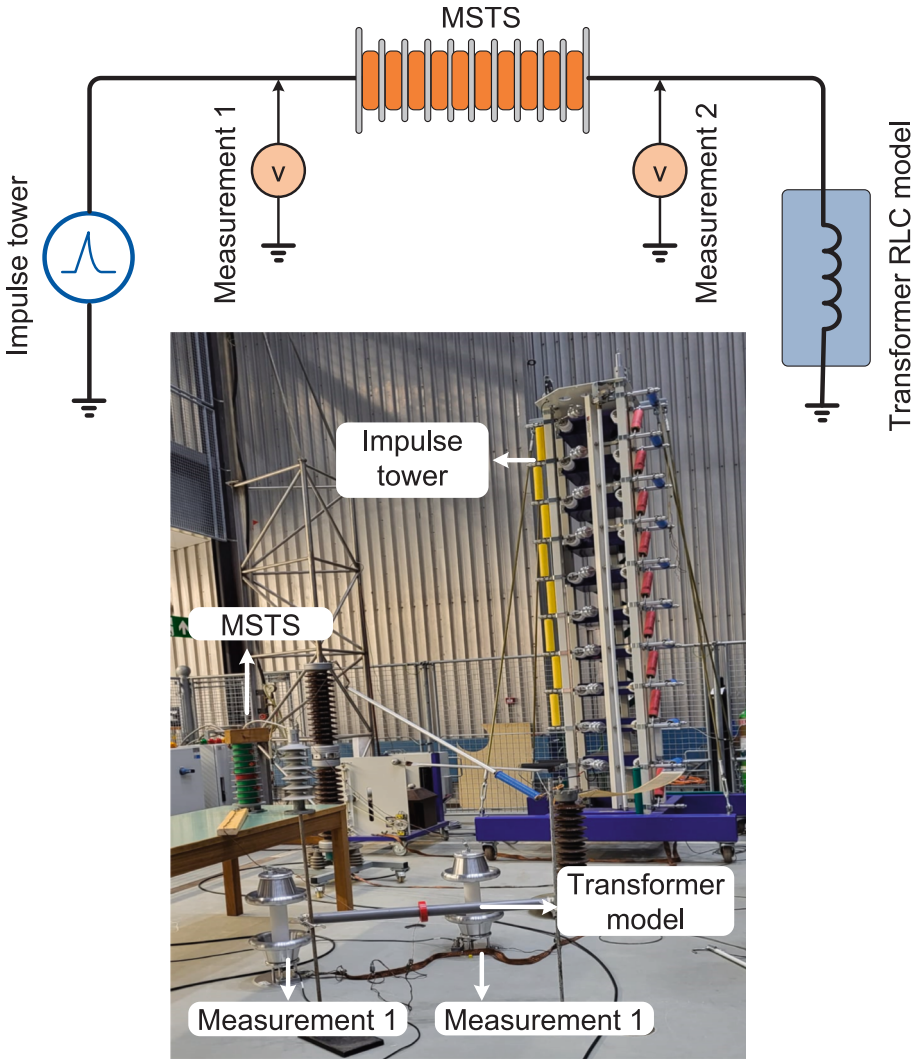

Fig. 15. Impulse HV test setup of MSTS.

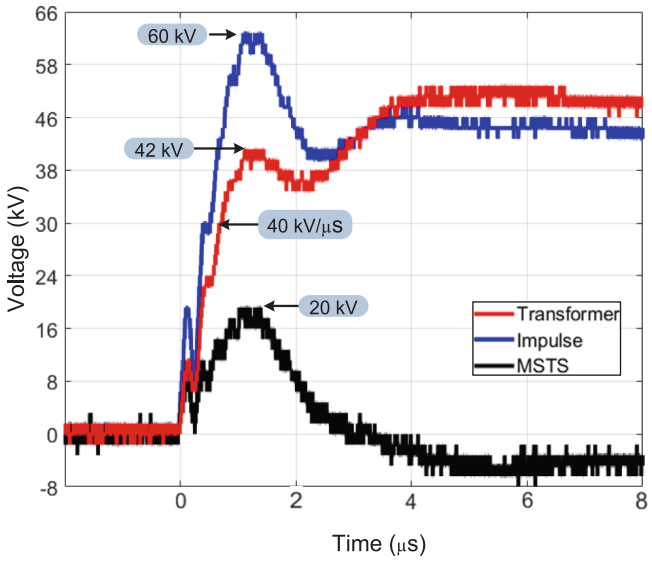

Fig. 16. Impulse test result of MSTS.

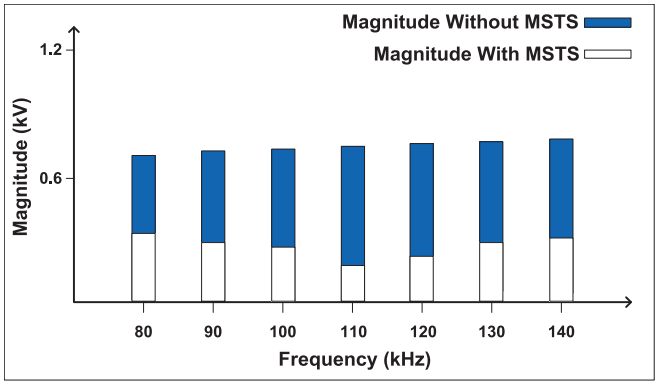

Fig. 17. Harmonic content of wind farm transformer voltage with and without the MSTS operation.

A multilayer scheme was implemented to address this issue, utilizing three layers to distribute the magnetic flux density. The data for each layer is presented in Table 3. As shown in Fig. 12 (b), the thickness of the saturation region near the wire is reduced to approximately 1 mm. The inductance of each module before being saturated remains around 72 μH, and after saturation, it decreases slightly to 71 μH. Therefore, the multilayer design of the MSTS modules significantly improves the device's performance and effectively manages saturation concerns in this protection device.

5. The MSTS experimental validation

This section aims to comprehensively evaluate the technical performance of the MSTS device for the frequency and time domains. The results of the designed MSTS closely align with those of the simulated model, with data used from Tables 1 and 3, respectively. The laboratory test results are divided into two scenarios, as follows.

5.1. Frequency sweep evaluation

In the first test scenario, the impedance of the designed MSTS is measured using the frequency sweep method. A vector network analyzer (VNA), model Omicron Bode 100, is employed for the measurements, covering a frequency range from 50 Hz to 10 MHz. The test setup, illustrated in Fig. 13, is designed to take into account the frequency response impedance of the MSTS.

In the laboratory test, the impedance of each module and the MSTS terminal is measured, with the results shown in Fig. 14. It can be seen that the maximum impedance of the MSTS reaches 700 Ω near the resonance frequency of 110 kHz. Additionally, the first resonance of each module occurs between 85 and 150 kHz, with peak impedance values ranging from 70 to 100 Ω. It is proven from this test that the total impedance of the MSTS is almost the sum of the impedances of the modules.

The main outcome of this test is the measurement of the MSTS impedance near the resonance frequency of the studied transformer. The experimental results are consistent with the simulated results obtained from the EMTP-based MSTS model, as shown in Fig. 8.

5.2. High voltage impulse test evaluation

The MSTS impulse evaluation test setup is presented in Fig. 15. The designed MSTS is connected in series to the wind farm transformer terminal (which is represented by an RLC circuit) and an impulse generator. The resonance frequency of the wind farm transformer model is considered 110 kHz. Furthermore, the maximum voltage of the impulse tower is 60 kV, while reaching this maximum magnitude within 1.2 μs declines to 50 % of the maximum magnitude of the transient magnitude in 50 μS. This setup consists of two fast measurement high voltage probes, which work based on the RC voltage division. The first probe is connected to an impulse generator terminal, and the next probe is connected to the wind farm transformer terminal. Hence, by subtracting the measured voltages, the voltage drop of the MSTS can be determined.

The results of the laboratory test setup are shown in Fig. 16. This plot includes the impulse generator voltage (blue curve), wind farm transformer terminal voltage (red curve), and the voltage drop across the MSTS (black curve). Based on the obtained results, the peak voltage at the wind farm transformer decreases from 60 kV to 42 kV, with a voltage decline rate of 40 kV/μs. This reduction is due to the voltage drop across the MSTS, which reaches a peak value of 20 kV. The experimental results

Table 4
Comparison of MSTS features.

Features	MSTS	Choke [13]-[14]	Tuneable choke	Arrester [21]
Connection type	Series	Series	Series	Parallel
Operation frequency range	Tuneable in a wide range	Above 1 MHz	Tuneable for narrow frequency band	No frequency dependency
Provided impedance	This can be adjusted by the number of modules	Less than 1 kΩ	Less than 1 kΩ	Low shunt impedance only in the case of overvoltage
Saturation possibility	This can be avoided by the multilayer design of the core	Mostly possible	Mostly possible	No ferromagnetic component
Voltage level	Both the distribution and transmission system	Distribution system	Distribution system	Both distribution and transmission system
Wind farm transformer internal resonance protection	Yes	Yes	Yes	No
Need for grounding	No	No	No	Yes

are validated by EMTP simulation, as shown in Fig. 9.

From the perspective of the voltage drop across the MSTS structure, this equipment provides adequate wind farm transformer protection at transmission voltage levels. Despite the MSTS being a prototype design, it can withstand a voltage drop of 60 kV, considering its modular design. This voltage is distributed across the ten modules of the MSTS, and by assuming a nearly linear distribution, each module experiences approximately 6 kV. For this, if the voltage level is suitable, it is straightforward to design the necessary insulation. Additionally, it is possible to increase the number of modules for higher voltage levels, which is convenient for tuning the MSTS for different protection levels.

By applying a fast Fourier transform (FFT) for the impulse generator signal and the wind farm transformer voltage for a wind farm transformer's resonance frequency, it can be seen that the MSTS effectively suppresses the transient signal around the critical wind farm transformer resonance frequency. The result of this analysis is shown in Fig. 17, where it is clearly illustrated that the amount of frequency content near the wind farm transformer's resonance frequency (which is within the operating range of the MSTS) is reduced by approximately 70 %.

Additionally, this is the frequency at which the MSTS provides its highest impedance. This frequency-based evaluation highlights the MSTS's successful performance as a protection device, effectively mitigating harmful transient effects at the wind farm transformer's critical resonance frequency.

6. The MSTS advantages discussion based on comparison

To briefly discuss the overall features provided by the MSTS, the following points should be highlighted:

- The MSTS is a viable solution for protecting wind farm transformers against transient voltage signals. This issue is resolved because of its modular design, which makes it straightforward to withstand higher voltage by distributing it across the series modules.
- The MSTS can be tuned within a wide frequency range to protect the wind farm transformer around the critical resonance frequency. This feature is provided by using a frequency shift for each MSTS module by using secondary resonance capacitors.
- The other highlighted specification of the MSTS is the core design. Considering the multilayer design of the MSTS core, the magnetic flux is distributed and unified on the core, resulting in better performance of the MSTS, which is far from the saturation condition on the core.

The discussed features have been proven throughout this study. To clarify the advantages of the designed MSTS, Table 4 compares the features provided by the MSTS and the well-known protective choke [13,14] and surge arrester specifications [21], which is used as a wind farm transformer series protection device against the transient signal.

As highlighted in Table 4, the MSTS operates over a broader frequency range and can withstand higher voltage levels compared to traditional protective chokes. Furthermore, the MSTS features adjustable impedance and avoids saturation due to its modular design and multilayer core capabilities, which are not typically incorporated into conventional choke designs. This gives the MSTS a significant operational advantage.

Compared to surge arresters, the MSTS provides critical resonance frequency filtering, protecting the wind farm transformer from both terminal and internal resonance, which can lead to overvoltage conditions. In contrast, surge arresters allow the wind farm transformer to experience resonance-induced overvoltage before mitigating it by diverting a large current to the ground. In summary of this comparison study the main advantages of the MSTS over the state of the are briefly as follows:

- Tuneable impedance over a wide frequency range,
- Applicability to both distribution and transmission systems,
- Internal resonance suppression without grounding requirements,
- A multilayer core design to prevent saturation.

As additional explanation about the designed MSTS and its coordination with the available control system in the wind energy system, the MSTS operates within microseconds as a passive protection device, making real-time coordination with supervisory systems (For example, SCADA or WAMS) impractical during fault events. However, the integration of condition monitoring or post-event reporting features could be explored in future designs to enhance system-level awareness and maintenance planning.

7. Conclusion

This paper introduces a Modular Series Transient Suppressor (MSTS) as an advanced protection device for wind farm transformers in modern power grids. The MSTS incorporates a modular design, adjustable resonance-shifting capacitors, and multilayer cores, significantly enhancing its capability to mitigate transient phenomena.

Simulation and experimental results demonstrate that the MSTS reduces peak transient signals by 30 %, decreases the voltage rise rate by 34 %, and suppresses harmonic content at critical resonance frequencies by 70 %. Its modular architecture ensures high-voltage endurance and facilitates maintenance, while the multilayer core effectively prevents magnetic saturation.

CRediT authorship contribution statement

Amir Heidary: Writing – original draft, Methodology, Investigation, Formal analysis, Data curation, Conceptualization. **Mohamad Ghaffarian Niasar:** Writing – review & editing, Validation, Supervision, Resources. **Marjan Popov:** Writing – review & editing, Validation, Supervision, Resources, Project administration.

Declaration of competing interest

The authors declare that they have no known competing financial interests or personal relationships that could have appeared to influence the work reported in this paper.

Acknowledgment

This work was financially supported by the Nederlandse Organisatie voor Wetenschappelijk Onderzoek (NWO) in collaboration with Transmission System Operator (TSO) TenneT, Distribution System Operator (DSO) Alliander, Royal SMIT Transformers, and TSO National Grid, U. K., in the Framework of the NWO-Toegepaste en Technische Wetenschappen (TTW) Project "Protection of Future Power System Components" under Grant 18.699.

Data availability

Data will be made available on request.

References

[1] Paap GC, Alkema AA, Van der Sluis L. Overvoltages in power transformers caused by no-load switching. IEEE Trans Power Delivery Jan. 1995;10(1):301–7.
[2] Yasuda Y, Uno N, Kobayashi H, Funabashi T. Surge Analysis on Wind Farm When Winter Lightning Strikes. IEEE Transactions on Energy Conversion March 2008;23 (1):257–62. https://doi.org/10.1109/TEC.2007.905361.
[3] Soloot AH, Høidalen HK, Gustavsen B. Influence of the winding design of wind turbine transformers for resonant overvoltage vulnerability. IEEE Trans Dielectr Electr Insul April 2015;22(2):1250–7.
[4] Abdulahović T, Thiringer T. Voltage Stress in a Transformer Winding During Very Fast Transients Caused by Breaker Closing Event. IEEE Trans Power Delivery Aug. 2014;29(4):1946–54.

[5] Akiki P, Xémard A, Trouilloud C, Chanelière J. Study of high frequency transient overvoltage caused by cable-transformer quarter-wave resonance. Electr Pow Syst Res 2021;197:0378–7796.
[6] Firouzi M, Gharehpetian GB. Improving Fault Ride-Through Capability of Fixed-Speed Wind Turbine by Using Bridge-Type Fault Current Limiter. IEEE Trans Energy Convers June 2013;28(2):361–9.
[7] Heidary A, Niasar MG, Popov M, Lekić A. Transformer Resonance: Reasons, Modeling Approaches, Solutions. IEEE Access 2023;11:58692–704.
[8] T. Dionise and S. Johnston, "Surge Protection for Ladle Melt Furnaces: LMF Transformer Terminals were Equipped with Primary Surge Protection Consisting of Surge Arresters and RC Snubbers," IEEE Industry Applications Magazine, vol. 21, no. 5, pp. 43-52, Sept.-Oct. 2015.
[9] Zinc Oxide RC-Surge Suppressor (ZORC) Capacitors, for HV-Motor and Transformers, https://www. vishay.com.
[10] K. Munji, "Design and validation of pre-insertion resistor rating for mitigation of zero missing phenomenon", In International conference on power systems transients (IPST2017), pp. 26-29.
[11] Heiermeier H, Raysaha RB. Power Testing of Preinsertion Resistors: Limitations and Solution. IEEE Trans Power Delivery Aug. 2017;32(4):1688–95.
[12] Korobeynikov SM, Krivosheev SI, Magazinov SG, Loman VA, Ya N. Suppression of Incoming High-Frequency Overvoltage in Transformer Coils. IEEE Trans Power Delivery Oct. 2021;36(5):2988–94.
[13] D. Smugala, Distribution transformers protection against High Frequency Switching Transients, PRZEGLĄD ELEKTROTECHNICZNY (Electrical Review), ISSN 0033-2097, R. 88 NR 5a, 2012.
[14] Smugała D, et al. New approach to protecting transformers against high frequency transients–wind turbine case study. Prz. Elektrotech 2013;89:186–90.
[15] D. Smugala, et al., "Very fast transient suppressing device," United States patent, US 8,929,048B2, 2015.
[16] Nasirpour F, Heidary A, Ghaffarian Niasar M, Popov M. High-frequency transformer winding model with adequate protection. Electr Pow Syst Res 2023;1 (223):109637.
[17] Heidary A, Ghaffarian Niasar M, Popov M. Comprehensive Evaluation of Toroid Ring Core Parallel Inductor and Resistor as a Transformer Protection Device. IEEE Transactions on Circuits and Systems I: Regular Papers, Sept. 2024;71(9): 4298–308.
[18] Zhou L, Huang L, Wei R, Wang D. A Novel Lightning Overvoltage Protection Scheme Using Magnetic Rings for Transmission Line Systems. IEEE Trans Ind Electron 2023;70(12):12872–82.
[19] W. Piasecki, G. Bywalec, M. Florkowski, M. Fulczyk, and J. Furgal, "New approach towards very fast transients suppression," Proceedings of IPST, 2007.
[20] Heidary A, Niasar MG, Popov M. Series magnetic coupled reactor saturation considerations for high voltage AC and DC power systems. Int J Electr Power Energy Syst 2024;1(158):109909.
[21] Zhang Y, Yang Q, Xie S, Zhang C. Mechanism and Application of Arrester Block Voltage Division to Lightning Transient Voltage Monitoring in Substation Transformers. IEEE Trans Electromagn Compat June 2019;61(3):689–96.